

Electronic correlations in the iron pnictides

M. M. Qazilbash,^{1,*} J. J. Hamlin,¹ R. E. Baumbach,¹ Lijun Zhang,² D. J. Singh,² M. B. Maple,¹ and D. N. Basov¹

¹ *Physics Department, University of California-San Diego, La Jolla, California 92093, USA.*

² *Materials Science and Technology Division, Oak Ridge National Laboratory, Oak Ridge, Tennessee 37831, USA.*

(Dated: November 3, 2018)

I. TEXT

In correlated metals derived from Mott insulators, the motion of an electron is impeded by Coulomb repulsion due to other electrons. This phenomenon causes a substantial reduction in the electron's kinetic energy leading to remarkable experimental manifestations in optical spectroscopy.¹ The high- T_c superconducting cuprates are perhaps the most studied examples of such correlated metals. The occurrence of high- T_c superconductivity in the iron pnictides^{2,3,4} puts a spotlight on the relevance of correlation effects in these materials.^{5,6,7} Here we present an infrared and optical study on single crystals of the iron pnictide superconductor LaFePO. We find clear evidence of electronic correlations in metallic LaFePO with the kinetic energy of the electrons reduced to half of that predicted by band theory of nearly free electrons. Hallmarks of strong electronic many-body effects reported here are important because the iron pnictides expose a new pathway towards a correlated electron state that does not explicitly involve the Mott transition.

The recent discovery of superconductivity in the iron pnictides promises to be an important milestone in condensed-matter physics.^{2,3} Here is a new class of materials with a layered structure and relatively high superconducting T_c values^{3,4} rivalling the doped cuprates. Electronic conduction is believed to occur in the iron-pnictogen layers,⁸ similar to the cuprates where the charge carriers are delocalized in the copper-oxygen planes. Two decades of research on the cuprates has established that a proper account of the exotic normal state properties is a prerequisite for the understanding of the superconducting instability.⁹ Thus motivated, we investigated the normal state of the iron pnictide superconductors with infrared and optical spectroscopy, focusing on charge dynamics in the conducting planes.

An optical experiment measures the dynamical response of the electron subjected to an external electromagnetic field and facilitates monitoring of many-body effects experienced by the electron in a material. These many-body effects include the interaction of the electron with other electrons, phonons as well as ordered or fluctuating spins. In Fig. 1a we display the real part of the ab -plane optical conductivity $\sigma_1(\omega)$ of LaFePO over a broad frequency range. Sample growth and characterization procedures, and the experimental details for obtain-

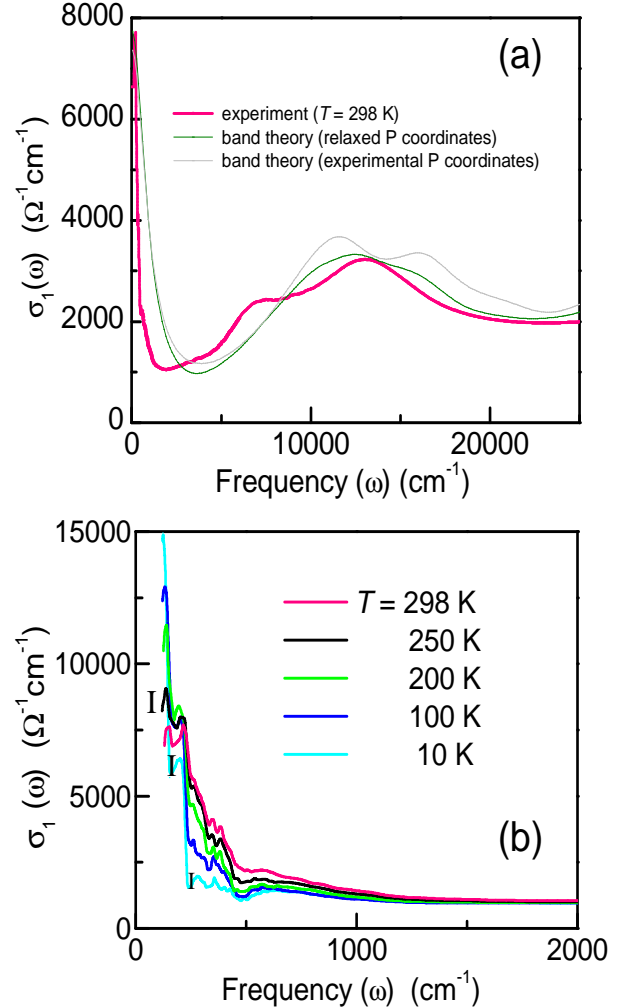


FIG. 1: (a) Real part of the ab -plane optical conductivity $\sigma_1(\omega)$ of LaFePO is plotted as a function of frequency for $T = 298$ K. Also shown are $\sigma_1(\omega)$ plots calculated within band theory. (b) Systematic temperature dependence of $\sigma_1(\omega)$. The uncertainty in $\sigma_1(\omega)$ in panel (b) is less than or equal to the thickness of the lines for $\omega > 350$ cm^{-1} . However, the uncertainty in $\sigma_1(\omega)$ increases at lower frequencies as indicated by the error bars.

ing the optical conductivity are provided in Methods and Supporting Information. The low frequency infrared response is dominated by the narrow Drude feature signifying the presence of itinerant charge carriers. Two distinct interband transitions in the form of hump-like structures are seen at higher frequencies. The temperature dependence of the Drude feature is displayed in Fig. 1b. The

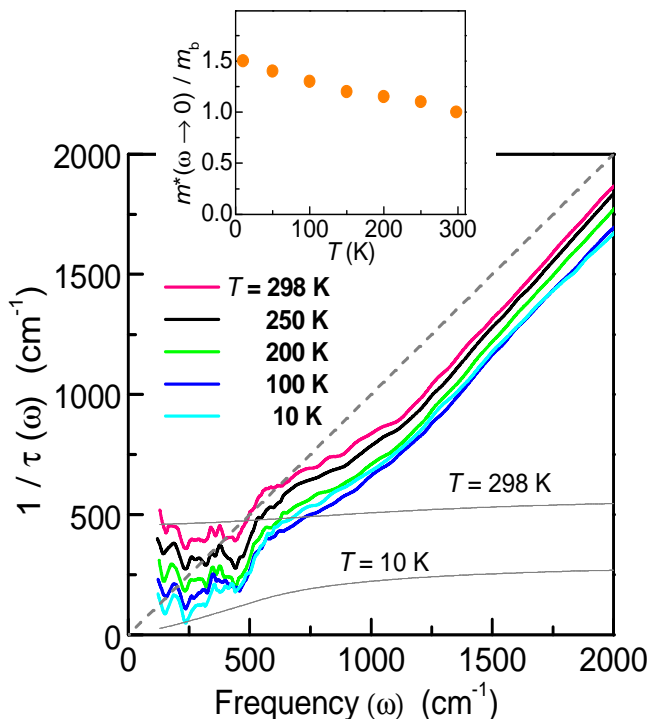


FIG. 2: The frequency dependence of the scattering rate $1/\tau(\omega)$ is plotted for representative temperatures in the normal state of LaFePO. The dashed line represents the equation $\omega = 1/\tau(\omega)$. The thin solid lines are the expected electron-phonon scattering rate at $T = 298$ K and $T = 10$ K calculated using a model phonon spectral density for LaFePO (see Supporting Information). The inset shows the temperature dependence of the mass enhancement factor in the low frequency limit $m^*(\omega \rightarrow 0)/m_b$.

Drude peak at low frequencies becomes sharper, and the conductivity at the lowest measured frequencies increases with decreasing temperature which is typical metallic behavior.

In order to gain insight into the effect of many-body interactions on the itinerant behavior of the charge carriers, we performed the extended Drude analysis¹⁰. Via the extended Drude analysis, we extract the scattering rate $1/\tau(\omega)$ and the mass enhancement factor $m^*(\omega)/m_b$ (see Supporting Information). The temperature dependence of $1/\tau(\omega)$ and $m^*(\omega \rightarrow 0)/m_b$ is respectively plotted in Fig. 2 and the inset. One can see that the scattering rate increases continuously and monotonically with frequency. Electron-phonon scattering theory predicts a constant, frequency-independent scattering rate above the cutoff of the phonon spectrum^{10,11}. Measurements and calculations of the phonon spectral density for LaFePO are not yet available. However, the cutoff is not likely to exceed 550 cm^{-1} inferred from calculations on the iron oxy-arsenides^{12,13}. Therefore, the absence of saturation of $1/\tau(\omega)$ at higher frequencies in LaFePO suggests that in addition to electron-phonon scattering, there are other scattering channel(s) arising from electronic and spin cor-

relations. It is interesting to note that the scattering rate has a linear frequency dependence between 1100 cm^{-1} and 2000 cm^{-1} and it deviates from linearity below 1100 cm^{-1} . This frequency dependence almost mimics the temperature dependence of the resistivity which has a linear temperature dependence at higher temperatures and a quadratic temperature dependence at low temperatures.¹⁴

At $T = 10$ K, the frequency dependent scattering rate lies below the line $\omega = 1/\tau(\omega)$ at low frequencies, signifying the presence of coherent quasiparticles. This is consistent with the observation of deHaas-vanAlphen oscillations in LaFePO.¹⁵ Note, however, that $1/\tau(\omega)$ is of the order of the excitation energy (frequency) at high energies (frequencies) even at low temperatures. This is significant since quasiparticles may be well-defined only near the Fermi energy whereas at higher energies we are dealing with a strongly dissipative system. At higher temperatures, $1/\tau(\omega)$ approaches the line $\omega = 1/\tau(\omega)$ i.e. the incoherent regime. In doped iron-arsenides, the scattering rate exceeds the excitation frequency,¹⁶ implying that transport in the iron-arsenides is more incoherent than in its phosphorous based counterparts. We note that the mass enhancement in the zero frequency limit due to low energy many-body interactions is at most 1.5 (inset of Fig. 2). This value of the mass enhancement is obtained using the experimentally determined plasma frequency which is already renormalized by high energy electronic correlations (see subsequent discussion and Supporting Information). Therefore, the mass enhancement obtained from the extended Drude analysis is a result of low energy many-body interactions. On the other hand, we find that high energy electronic correlations lead to an effective mass renormalization in LaFePO by a factor of 2 which is equivalent to a kinetic energy reduction by a factor of 2 compared to the band theory value which we discuss next.

With itinerant nature of LaFePO firmly identified by our data in Figs.1 and 2, we now proceed to the central part of our analysis pertaining to the electronic kinetic energy. The optical conductivity data provides a measure of the kinetic energy K of the electrons.¹ The kinetic energy can also be readily evaluated using band structure calculations. As a rule, experimental results for itinerant electron systems are in good agreement with the band structure calculations leading to K_{exp}/K_{band} close to unity in simple metals (see Fig. 3). However, interesting electronic effects due to strong interactions involving charge, spin and orbital degrees of freedom occurring in many intermetallic compounds with d - (and f -) electrons yield dynamical effects beyond ordinary band structure results. All these effects compete with itinerancy of electrons leading to the suppression of K_{exp}/K_{band} value from unity. The most notorious example is a Mott insulator where $K_{exp} = 0$ due to Coulomb repulsion whereas band structure results still predict metallic response with finite K_{band} . A trend revealed by metals in the vicinity of Mott insulators is that K_{exp}/K_{band} increases from zero to

finite values as Coulomb correlations are suppressed resulting in a Mott insulator-to-metal transition with doping or temperature (Fig.3). While K_{exp}/K_{band} in correlated metals derived from Mott insulators is finite, it is significantly less than unity. Therefore optical experiments in tandem with band structure results offer reliable means to probe electronic correlations in materials.

We have calculated $\sigma_1(\omega)$ from band theory within the generalized gradient approximation (GGA) using both experimental and relaxed coordinates (see Fig. 1a and Supporting Information). The calculated $\sigma_1(\omega)$ shows a Drude feature at low frequencies and higher frequency interband transitions, in reasonable agreement with the experimental data. The band theory calculations show that LaFePO is a metal in agreement with experiment. There are, however, some differences between the calculated and measured $\sigma_1(\omega)$ that will be elaborated in subsequent paragraphs. We note here that GGA calculations were performed with two choices of the atomic coordinates. The two choices do not significantly affect the Drude part but do affect the peak positions of the interband transitions.

We now wish to draw attention to the key parameter associated with the optical conductivity - the area under the Drude part of $\sigma_1(\omega)$ which is proportional to the electron's kinetic energy. One can immediately see in Fig. 1a that the area under the Drude part of the measured $\sigma_1(\omega)$ is significantly less than that calculated within band theory. To put this on a quantitative footing, we define the experimental kinetic energy as:¹⁷

$$K_{exp}(\omega_c) = \frac{\hbar c_0}{e^2} \int_0^{\omega_c} \frac{2\hbar}{\pi} \sigma_1(\omega) d\omega \quad (1)$$

In the above equation, c_0 is the distance between the FeP planes. Upon integrating the Drude part of the experimental $\sigma_1(\omega)$ up to a cutoff frequency $\omega_c = 3000 \text{ cm}^{-1}$, we obtain a kinetic energy $K_{exp} = 0.15 \text{ eV}$. The theoretical value of the kinetic energy is obtained directly from band theory calculations of the plasma frequency, which give $K_{band} = 0.29 \text{ eV}$ (see Supporting Information for details). K_{exp} is nearly 50% of K_{band} and this reduction is due to correlation effects not accounted in band theory. We note that this discrepancy between K_{exp} and K_{band} is robust with respect to the uncertainties in the experimental and theoretical values of the kinetic energy which are discussed in the Methods section and Supporting Information. Furthermore, our findings are in agreement with a recent photoemission experiment in which the measured bandwidth is nearly half of that calculated within band theory.¹⁸

Among the various superconducting iron-pnictide families, LaFePO has one of the highest normal state conductivities. Despite the high conductivity, the reduction of the kinetic energy is significant. Therefore, the ground state wave-function of LaFePO is not the same as calculated by band theory, and dynamical correlation effects omitted by band theory have to be taken into account for

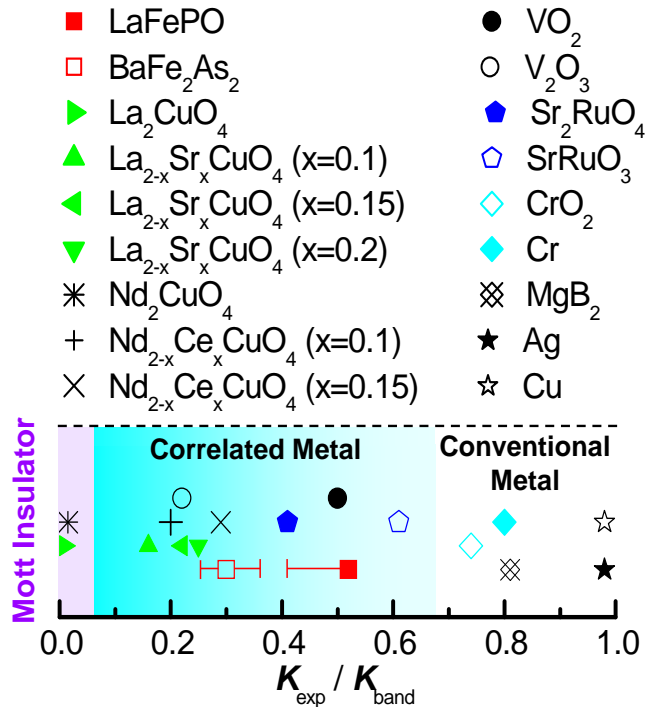


FIG. 3: The ratio of the experimental kinetic energy and the kinetic energy from band theory K_{exp}/K_{band} for the iron pnictides and various other metals is plotted. The data points are offset in the vertical direction for clarity. The value of the LaFePO data point and the associated error bar are discussed in the text, Methods section and the Supporting Information. The values K_{exp} and K_{band} are obtained from the following references: paramagnetic BaFe₂As₂ (Refs.19,20,21), La_{2-x}Sr_xCuO₄ (Ref.22), Nd_{2-x}Ce_xCuO₄ (Ref.22), VO₂ rutile metal (Ref.11), V₂O₃ paramagnetic metal (Refs.23,24), Sr₂RuO₄ (Refs.25,26), paramagnetic SrRuO₃ (Refs.27,28), half-metallic CrO₂ (Refs.29,30,31), paramagnetic Cr (Ref.32), MgB₂ (*a*-axis) (Ref.33), Ag and Cu (Ref.34). The error bar on the BaFe₂As₂ data point is based on the scatter in the theory and experimental values of the plasma frequency (Ref.19,20,21). The error bars (not shown) for other materials are estimated to be at least the width of the symbols and at most ± 0.05 .

a realistic theoretical description. This view is further supported by the differences between the measured optical interband transitions and those derived from the band structure (see Fig. 1a). In the experimental data, there are two distinct peaks in $\sigma_1(\omega)$ centered at 7200 cm^{-1} and 13000 cm^{-1} , most likely arising from optical transitions between the Fe-3*d* bands. We note that the band theory calculations predict two peaks between 10000 and 17000 cm^{-1} whose positions are sensitive to the atomic coordinates. The discrepancy between the experimental data and band structure calculations are likely due to modification of the actual band structure arising from electronic correlations.

The reduction of the kinetic energy compared to band theory in LaFePO, its proximity to the incoherent metal

regime, and the absence of a Mott insulator in its phase diagram inspired us to compare it to other exotic conductors that have been studied in the past. Fig 3 is a map showing the location of various exotic conductors as well as a few conventional metals (Ag and Cu) based upon the ratio of the experimental kinetic energy to that calculated within band theory. The exotic conductors that have been selected for comparison share at least one of the following features in common with the iron-pnictides: high- T_c superconductivity, itinerant magnetism, and/or electronic correlations. Within the ambit of Fig 3, the correlated metal regime is characterized by a substantially reduced empirical kinetic energy of charge carriers compared to theory. Note that electron-phonon coupling does not result in a significant reduction of the electron's kinetic energy (unless it is extremely strong as to lead to polaron formation).¹ Electron-phonon coupling in MgB₂ superconductor, for example, results in K_{exp}/K_{band} not much less than unity in the metallic state (Fig.3).

We now look at the consequences of magnetic interactions on the kinetic energy. In paramagnetic Cr and half-metallic CrO₂, two classic systems with itinerant magnetism, spin correlations lead to 20-25% reduction in K_{exp} relative to K_{band} (Fig.3). Moreover, in the cuprates where the magnetism has local moment character, opposite to the itinerant case discussed above, magnetic interactions also lead to a relatively small reduction in the electron's kinetic energy compared to that predicted by band theory.²² Even where it is argued that the role of magnetic interactions in the cuprates is important, it is seen that 80-90% of the experimental reduction in kinetic energy compared to band theory is accounted for by the intra-atomic Coulomb repulsion and 10-20% may be attributed to antiferromagnetic correlations.²² It is worth emphasizing that K_{exp} is reduced substantially compared to K_{band} in the cuprates, oxides of vanadium and the ruthenate family of metals as shown in Fig.3 - these materials have Mott insulators in their phase diagrams and dynamical Coulomb correlations dominate transport behavior in the metallic states. Thus, intra-atomic Coulomb repulsion is one established mechanism that leads to a substantial reduction in K_{exp} compared to K_{band} .

We note that the parent compounds of the superconducting iron-arsenides exhibit magnetic ordering at low temperatures,³⁵ but they remain metallic and are not insulating in the ordered state. Furthermore, LaFePO shows no signs of magnetic ordering³⁶ or insulating behavior.¹⁴ However, spin correlations likely exist in LaFePO and the paramagnetic phases of the iron arsenides.¹² The data in Fig 3 show that both in LaFePO and paramagnetic BaFe₂As₂, K_{exp}/K_{band} is less than that in other typical itinerant magnets and is substantially less than unity. Notice that K_{exp}/K_{band} is further reduced for paramagnetic BaFe₂As₂ compared to LaFePO which means that the arsenides are even more correlated than the phosphides.⁵ These observations may not be explained by spin correlations alone, in which case

they signify the relevance of dynamical Coulomb correlations to the physics of the iron pnictides. This is remarkable in the absence of a Mott transition in their phase diagrams. Therefore, the iron pnictides are properly classified as being in the moderate correlation regime with the on-site Coulomb repulsion of the order of the bandwidth. There is the possibility that complexity related to charge, magnetic and orbital degrees of freedom leads to a correlated metal that need not be derived from a Mott insulator. Our results demonstrate that transport in the iron-pnictides lies between the band-like itinerant and the Mott-like local magnetic moment extremes.

II. METHODS

The growth and characterization procedures for LaFePO single crystals are given in Ref. 14. Resistivity and magnetization measurements reveal a superconducting T_c of ≈ 6 K, with complete zero-field-cooled diamagnetic shielding in the superconducting state. The crystals are platelets, typically 0.5 mm \times 0.5 mm \times 0.05 mm in size.

The *ab*-plane reflectance was measured in the near-normal incidence geometry in a Bruker v66 Infrared Fourier-transform Spectrometer at frequencies between 100 cm⁻¹ and 24000 cm⁻¹. The reflectance measurements were performed at the following temperatures: 298 K, 250 K, 200 K, 150 K, 100 K, 50 K, and 10 K. We obtained the optical constants through fitting the reflectance data with Drude and Lorentzian oscillators, and Kramers-Kronig constrained variational dielectric functions as described in Ref. 37. In addition, variable-angle spectroscopic ellipsometry was performed in the frequency range 5500 - 25000 cm⁻¹ which improves the accuracy of the extracted optical constants in this frequency range. The temperature dependence of the *ab*-plane reflectance of LaFePO crystals is displayed in Fig.S1 in the Supporting Information.

Details regarding the extended Drude analysis are given in Supporting Information online. We note here that $K_{exp}/K_{band} = 0.52$ for LaFePO plotted in Fig. 3 is an upper bound, and other methods for obtaining K_{exp}/K_{band} give a lower bound of 0.4. Further details about calculations of K_{exp} and K_{band} for LaFePO are given in the Supporting Information. Also included in the Supporting Information are calculations of the scattering rates due to electron-phonon coupling and some notes on Fig. 3.

III. ACKNOWLEDGEMENTS

The authors are grateful to Elihu Abrahams, A. V. Boris, A. V. Chubukov, A. J. Millis, Oleg Shpyrko, Qimiao Si, and Congjun Wu for discussions. M.M.Q. thanks A. Kuzmenko for assistance with the software for infrared data analysis. This work was supported in part

by the National Science Foundation grant NSF DMR 0705171.

-
- * E-mail: mumtaz@physics.ucsd.edu
- ¹ Millis, A. J. in *Strong Interactions in Low Dimensions*, (eds Baeriswyl, D. & Degiorgi, L.), Kluwer Academic Publishers, Dordrecht, The Netherlands (2004).
 - ² Kamihara, Y. *et al.* Iron-based layered superconductor: LaOFeP. *J. Am. Chem. Soc.* **128**, 10012-10013 (2006).
 - ³ Kamihara, Y., Watanabe, T., Hirano, M. & Hosono, H. Iron-based layered superconductor LaO_{1-x}F_xFeAs (x = 0.05-0.12) with T_c = 26 K. *J. Am. Chem. Soc.* **130**, 3296-3297 (2008).
 - ⁴ Ren, Z.-A. *et al.* Superconductivity at 55 K in Iron-based F-doped layered quaternary compound SmO_{1-x}F_xFeAs. *Chin. Phys. Lett.* **25**, 2215-2216 (2008).
 - ⁵ Si, Q. & Abrahams, E. Strong correlations and magnetic frustration in the high T_c iron pnictides. *Phys. Rev. Lett.* **101**, 076401 (2008).
 - ⁶ Haule, K., Shim, J. H. & Kotliar, G. Correlated electronic structure of LaO_{1-x}F_xFeAs. *Phys. Rev. Lett.* **100**, 226402 (2008).
 - ⁷ Laad, M. S., Craco, L., Leoni, S. & Rosner, H. Electrodynamic response of incoherent metals: Normal phase of iron pnictides. *Phys. Rev. B* **79**, 024515 (2009).
 - ⁸ Kamihara, Y. *et al.* Electromagnetic properties and electronic structure of the iron-based layered superconductor LaFePO. *Phys. Rev. B* **77**, 214515 (2008).
 - ⁹ Bonn, D. A. Are high-temperature superconductors exotic? *Nat. Phys.* **2**, 159-168 (2006).
 - ¹⁰ Basov, D. N. & Timusk, T. Electrodynamics of high-T_c superconductors. *Rev. Mod. Phys.* **77**, 721-779 (2005).
 - ¹¹ Qazilbash, M. M. *et al.* Correlated metallic state of vanadium dioxide. *Phys. Rev. B* **74**, 205118 (2006).
 - ¹² Singh, D. J. & Du, M.-H. Density functional study of LaFeAsO_{1-x}F_x: A low carrier density superconductor near itinerant magnetism. *Phys. Rev. Lett.* **100**, 237003 (2008).
 - ¹³ Boeri, L., Dolgov, O. V. & Golubov, A. A. Is LaFeAsO_{1-x}F_x an electron-phonon superconductor? *Phys. Rev. Lett.* **101**, 026403 (2008).
 - ¹⁴ Hamlin, J. J., Baumbach, R. E., Zocco D. A., Sayles, T. A. & Maple, M. B. Superconductivity in single crystals of LaFePO. *J. Phys.: Condens. Matter* **20**, 365220 (2008).
 - ¹⁵ Coldea, A. I. *et al.* Fermi surface of superconducting LaFePO determined from quantum oscillations. *Phys. Rev. Lett.* **101**, 216402 (2008).
 - ¹⁶ Yang, J. *et al.*, arXiv:0807.1040.
 - ¹⁷ Millis, A. J., Zimmers, A., Lobo, R. P. S. M., Bontemps, N. & Homes, C. C. Mott physics and the optical conductivity of electron-doped cuprates. *Phys. Rev. B* **72**, 224517 (2005).
 - ¹⁸ Lu, D. H. *et al.* Electronic structure of the iron-based superconductor LaOFeP. *Nature* **455**, 81-84 (2008).
 - ¹⁹ Hu, W. Z. *et al.* Origin of the spin density wave instability in AFe₂As₂ (A = Ba, Sr) as revealed by optical spectroscopy. *Phys. Rev. Lett.* **101**, 257005 (2008).
 - ²⁰ Ma, F., Lu, Z.-Y. & Xiang, T., arXiv:0806.3526.
 - ²¹ Drechsler S.-L. *et al.* New insight into the physics of iron pnictides from optical and penetration depth data, arXiv:0904.0827.
 - ²² Comanac, A., De Medici, L., Capone, M. & Millis, A. J. Optical conductivity and the correlation strength of high-temperature copper-oxide superconductors. *Nat. Phys.* **4**, 287-290 (2008).
 - ²³ Thomas, G. A. *et al.* Optical properties of a correlated electron system. *J. Low Temp. Phys.* **95**, 33-38 (1994).
 - ²⁴ Rozenberg, M. J., Kotliar, G. & Kajueter, H. Transfer of spectral weight in spectroscopies of correlated electron systems. *Phys. Rev. B* **54**, 8452-8468 (1996).
 - ²⁵ Katsufuji, T., Kasai, M. & Tokura Y. In-plane and out-of-plane optical spectra of Sr₂RuO₄. *Phys. Rev. Lett.* **76**, 126-129 (1996).
 - ²⁶ Singh, D. J. Relationship of Sr₂RuO₄ to the layered superconducting cuprates. *Phys. Rev. B* **52**, 1358-1361 (1995).
 - ²⁷ Ahn, J. S. *et al.* Spectral evolution in (Ca,Sr)RuO₃ near the Mott-Hubbard transition, *Phys. Rev. Lett.* **82**, 5321-5324 (1999).
 - ²⁸ Mazin, I. I. & Singh D. J. Electronic structure and magnetism in Ru-based perovskites. *Phys. Rev. B* **56**, 2556-2571 (1997).
 - ²⁹ Singley, E. J., Weber, C. P., Basov, D. N., Barry, A. & Coey, J. M. D. Charge dynamics in the half-metallic ferromagnet CrO₂, *Phys. Rev. B* **60**, 4126-4130 (1999).
 - ³⁰ Lewis, S. P., Allen, P. B. & Sasaki, T. Band structure and transport properties of CrO₂. *Phys. Rev. B* **55**, 10253-10260 (1997).
 - ³¹ Mazin, I. I., Singh, D. J. & Ambrosch-Draxl, C. Transport, optical, and electronic properties of the half-metal CrO₂. *Phys. Rev. B* **59**, 411-418 (1999).
 - ³² Romaniello, P., de Boeij, P. L., Carbone, F. & van der Marel, D. Optical properties of bcc transition metals in the range 040 eV. *Phys. Rev. B* **73**, 075115 (2006).
 - ³³ Guritanu, V. *et al.* Anisotropic optical conductivity and two colors of MgB₂. *Phys. Rev. B* **73**, 104509 (2006).
 - ³⁴ Romaniello, P. & de Boeij, P. L. Time-dependent current-density-functional theory for the metallic response of solids. *Phys. Rev. B* **71**, 155108 (2005).
 - ³⁵ de la Cruz, C. *et al.* Magnetic order close to superconductivity in the iron-based layered LaO_{1-x}F_xFeAs systems. *Nature* **453**, 899-902 (2008).
 - ³⁶ Carlo, J. P. *et al.*, arXiv:0805.2186.
 - ³⁷ Kuzmenko, A. B. Kramers-Kronig constrained variational analysis of optical spectra. *Rev. Sci. Instrum.* **76**, 083108 (2005).

Electronic correlations in the iron pnictides

Supplementary Information

M. M. Qazilbash, J. J. Hamlin, R. E. Baumbach, Lijun Zhang, D. J. Singh, M. B. Maple, and D. N. Basov.

Reflectance Measurements

The temperature dependence of the *ab*-plane reflectance of LaFePO crystals is displayed in Fig.S1. This material is a metal as attested by the high values of the reflectance ($\geq 95\%$) at low frequencies. Two prominent hump-like features between 5000 cm^{-1} and 15000 cm^{-1} are due to interband transitions.

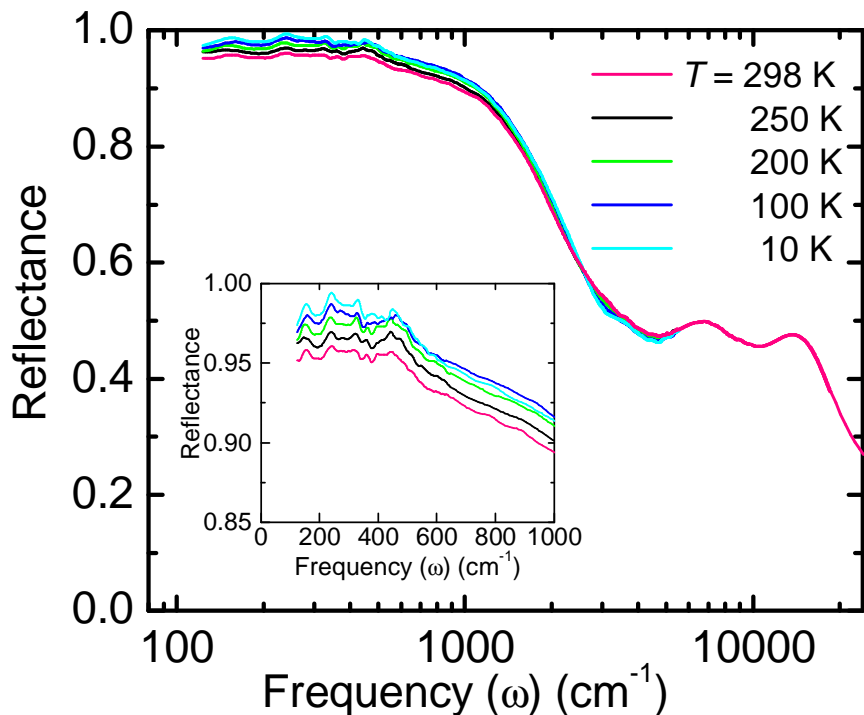


Fig. S1: Plots of *ab*-plane reflectance of single crystal LaFePO as a function of frequency for several representative temperatures. The inset shows magnified plots of the reflectance at low frequencies.

Extended Drude analysis

We calculate the scattering rate $1/\tau(\omega)$ and the mass enhancement factor $m^*(\omega)/m_b$ from the following equations [S1]:

$$\frac{1}{\tau}(\omega) = -\frac{\omega_p^2}{\omega} \text{Im} \left(\frac{1}{\tilde{\epsilon}(\omega) - \epsilon_H} \right), \quad (\text{A})$$

$$\frac{m^*(\omega)}{m_b} = -\frac{\omega_p^2}{\omega^2} \text{Re} \left(\frac{1}{\tilde{\epsilon}(\omega) - \epsilon_H} \right). \quad (\text{B})$$

In the above equations, $\tilde{\epsilon}(\omega) = \epsilon_1(\omega) + i\epsilon_2(\omega)$ is the complex dielectric function from which we subtract ϵ_H i.e. the contribution of interband transitions. Note that $\epsilon_H = 15$ for LaFePO and has negligibly small temperature dependence. The complex dielectric function is related to the complex optical conductivity $\tilde{\sigma}(\omega) = \sigma_1(\omega) + i\sigma_2(\omega)$ by the expression $\tilde{\epsilon}(\omega) = 1 + \frac{4\pi i}{\omega} \tilde{\sigma}(\omega)$. The plasma frequency $\omega_p = 14900 \text{ cm}^{-1}$ ($\approx 1.8 \text{ eV}$) is obtained from the experimental data via

$$\frac{\omega_p^2}{8} = \int_0^{\omega_c} \sigma_1(\omega) d\omega, \quad (\text{C})$$

with $\omega_c = 3000 \text{ cm}^{-1}$. With this choice of the plasma frequency, m_b is the renormalized band mass, and $m^*(\omega)/m_b$ gives the low energy mass enhancement in excess of that resulting from bandwidth renormalization (or kinetic energy reduction).

Calculations of K_{exp} and K_{band} for LaFePO

The experimental kinetic energy was obtained via Eq. 1 and is proportional to the area under the $\sigma_1(\omega)$ data at $T = 298 \text{ K}$ with a cutoff frequency $\omega_c = 3000 \text{ cm}^{-1}$. For the purpose of this calculation, we assume that $\sigma_1(\omega = 120 \text{ cm}^{-1})$ has this constant value down to zero frequency. This procedure leads to $K_{\text{exp}} / K_{\text{band}} = 0.52$ which is plotted in Fig. 3 and is an upper bound on this ratio. A cutoff frequency ω_c higher than 3000 cm^{-1} is inappropriate because it would clearly lead to contributions from interband transitions. This view is supported by the fact that the imaginary part of the conductivity $\sigma_2(\omega)$ has a zero crossing at $\omega \approx 3000 \text{ cm}^{-1}$. The contribution of itinerant carriers in the conduction bands to $\sigma_2(\omega)$ is positive while the negative contribution to $\sigma_2(\omega)$ from interband transitions leads to the zero crossing. Hence contribution of interband transitions to the real part of the conductivity $\sigma_1(\omega)$ will become non-negligible for frequencies above $\omega \approx 3000 \text{ cm}^{-1}$.

A lower cutoff $\omega_c = 1500 \text{ cm}^{-1}$ near the minimum in $\sigma_1(\omega)$ can be justified as well and will lead to $K_{\text{exp}} / K_{\text{band}} = 0.4$. A cutoff frequency less than 1500 cm^{-1} will underestimate K_{exp} . We also fit the optical conductivity to Drude and Lorentzian oscillators and obtained K_{exp} via the area under the Drude contribution to $\sigma_1(\omega)$. This procedure gives a ratio $K_{\text{exp}}/K_{\text{band}} = 0.42$. The two latter methods provide lower bounds on $K_{\text{exp}} / K_{\text{band}}$ that are depicted in Fig. 3 by the extent of the error bar. Moreover, the two latter methods only serve to strengthen our conclusions regarding the importance of correlations in LaFePO.

Calculations of the optical conductivity and plasma frequency were done using the GGA [S2] band structure as obtained in the full potential linearized augmented planewave method [S3,S4] as implemented in the Wien2k code (Blaha, P. *et al.*, Wien2k, <http://www.wien2k.at>). We used converged tested basis sets including local orbitals. The Brillouin zone sampling for the optical calculations was done using a very dense grid of more than 5000 k-points in the symmetry irreducible wedge. Calculations were done for two values of the P internal coordinate: that determined by energy minimization ($z_P=0.3780$; in a setting where the Fe is at $z_{\text{Fe}}=0.5$) and the reported experimental value ($z_P=0.3661$). The plasma frequency was obtained from the band velocities directly without broadening as shown below [S5,S6]:

$$\omega_{p,ii}^2 = \frac{4\pi e^2}{\hbar^2} \sum_n \int \frac{d\mathbf{k}}{V} v_{ii,n}^2(\mathbf{k}) \delta(\varepsilon_n(\mathbf{k}) - \varepsilon_F) \quad (\text{D})$$

For the tetragonal system here, ii corresponds to xx ($= yy$) and zz , n is band index, v is band velocity, and V is the normalization volume. The ab -plane plasma frequency $\omega_{p,xx} = 2.51 \text{ eV}$ for the experimental P coordinate, and $\omega_{p,xx} = 2.58 \text{ eV}$ for the relaxed P coordinate. These theoretical plasma frequency values are robust to about 1% with respect to a shift in the Fermi energy by 0.1 electrons per Fe (up and down). This is a consequence of the high density of states at the Fermi energy. Note that the band theory kinetic energy is directly proportional to the square of the calculated plasma frequency [S1,S6] with the constant of proportionality given by a combination of fundamental constants and the separation between the conducting planes c_0 :

$$K_{\text{band}} = \frac{c_0 \omega_{p,xx}^2}{120\pi e c} \quad (\text{E})$$

In the above equation, the kinetic energy and plasma frequency are in units of eV, and the other quantities are in SI units.

The calculated Drude and interband optical conductivities were broadened by 0.1 eV and 0.2 eV, respectively, and then added to produce the band theory optical conductivity plots shown in Fig.1a. The Drude peak is broadened by 0.1 eV in the theory so as to give the same conductivity in the $\omega \rightarrow 0$ limit as in the experimental data. Please note that the theoretical plasma frequency (and kinetic energy) is directly calculated using eq. D and is not affected by the numerical value of the broadening.

The calculated interband spectrum was broadened by 0.2 eV. This value was chosen to better compare with the shape of the experimental spectrum, including the width and height of peaks. We want to point out that this was done without completely smearing out the distinct interband features in the calculated spectrum.

Calculation of scattering rate due to electron-phonon coupling

We calculate $1/\tau(\omega)$ for electron-phonon scattering in LaFePO using eq.F below [S1]. We employ a constant Eliashberg function $\alpha^2F(\omega) = 0.1$ with lower and upper cutoff frequencies 50 cm^{-1} and 550 cm^{-1} respectively. This form mimics the phonon spectral density of LaFePO whose precise magnitude and form is not known at present while the upper cutoff frequency is estimated based on the calculations on the iron oxy-arsenides [S7,S8]. We note that the precise form of $\alpha^2F(\omega)$ does not affect the shape of the calculated $1/\tau(\omega)$ which saturates at frequencies higher than the upper cutoff frequency of the phonon spectrum. A constant temperature independent and frequency independent impurity scattering rate $1/\tau_{\text{imp}}(\omega) = 20 \text{ cm}^{-1}$ is used for LaFePO.

$$\frac{1}{\tau}(\omega, T) = \frac{1}{\tau_{\text{imp}}} + \frac{\pi}{\omega} \int_0^{\infty} d\Omega \alpha^2 F(\Omega) \left[2\omega \coth\left(\frac{\Omega}{2T}\right) - (\omega + \Omega) \coth\left(\frac{\omega + \Omega}{2T}\right) + (\omega - \Omega) \coth\left(\frac{\omega - \Omega}{2T}\right) \right] \quad (\text{F})$$

Notes on Fig.3

Values of K_{exp} and K_{band} for materials other than LaFePO were obtained from the references noted in the caption of Fig.3. The experimental values were obtained from infrared data obtained at room temperature for all materials except V_2O_3 ($T = 170 \text{ K}$) and rutile VO_2 ($T = 360 \text{ K}$). Note that the kinetic energy is proportional to the square of the plasma frequency. Therefore, the ratio $K_{\text{exp}}/K_{\text{band}}$ is identical to the ratio of the square of the experimental plasma frequency and the square of the band theory plasma frequency.

It will be interesting to see what the $K_{\text{exp}}/K_{\text{band}}$ ratios are for the electron- and hole-doped superconducting 122-iron arsenides. Evidence suggests that $K_{\text{exp}}/K_{\text{band}} \approx 0.3 - 0.4$ for these materials. For example, in $\text{Ba}_{0.55}\text{K}_{0.45}\text{Fe}_2\text{As}_2$ the best estimate of the empirical plasma frequency is 1.6 eV (Ref. S9) and an estimate of the band theory value is 2.63 eV (Ref. S10). This gives $K_{\text{exp}}/K_{\text{band}} = 0.37$ for $\text{Ba}_{0.55}\text{K}_{0.45}\text{Fe}_2\text{As}_2$. However, more infrared data on single crystals and detailed density functional calculations of the plasma frequencies are required for an accurate assessment of $K_{\text{exp}}/K_{\text{band}}$ in other doped 122-arsenides. Similarly, *ab*-plane infrared data on single crystals of 1111-iron arsenides (undoped and doped) are necessary to obtain reliable $K_{\text{exp}}/K_{\text{band}}$ ratios. It is expected that the 1111-iron arsenides are even more correlated than the 122-iron arsenides.

Two families of materials, the manganites and heavy fermion compounds were considered but not included in Fig.3. The infrared data in the doped manganites has not converged primarily because these materials are far more prone to phase separation than other correlated oxides. Heavy fermion materials are unique in that they are strongly correlated f -electron systems at low temperatures and are weakly interacting at higher temperatures. Heavy fermion systems at low temperatures exhibit mass enhancement (or kinetic energy reduction) by a factor of ~ 100 compared to the band mass [S6].

To conclude, we have shown in Fig. 3 that the degree of electronic correlations in a wide variety of materials can be determined by comparing the kinetic energy of the itinerant electrons in a system measured by optical experiments to the band theory kinetic energy which describes the same system in the weakly interacting regime.

-
- S1. Basov, D. N. & Timusk, T. Electrodynamics of high- T_c superconductors. *Rev. Mod. Phys.* **77**, 721-779 (2005).
- S2. Perdew, J. P., Burke, K. & Ernzerhof, M. Generalized gradient approximation made simple. *Phys. Rev Lett.* **77**, 3865-3868 (1996).
- S3. Singh, D. J. & Nordstrom, L. *Planewaves, pseudopotentials, and the LAPW Method*, 2nd Edition (Springer, Berlin, 2006).
- S4. Sjostedt, E., Nordstrom, L. & Singh, D. J. An alternative way of linearizing the augmented plane-wave method. *Solid State Commun.* **114**, 15-20 (2000).
- S5. Ashcroft, N. W. & Mermin, N. D. *Solid State Physics*, Saunders College Publishing, Harcourt Brace & Company, Orlando, Florida, (1976).
- S6. Millis, A. J. in *Strong Interactions in Low Dimensions*, (eds Baeriswyl, D. & Degiorgi, L.), Kluwer Academic Publishers, Dordrecht, The Netherlands (2004).
- S7. Singh, D. J. & Du, M.-H. Density functional study of $\text{LaFeAsO}_{1-x}\text{F}_x$: A low carrier density superconductor near itinerant magnetism. *Phys. Rev. Lett.* **100**, 237003 (2008).
- S8. Boeri, L., Dolgov, O. V. & Golubov, A. A. Is $\text{LaFeAsO}_{1-x}\text{F}_x$ an electron-phonon superconductor? *Phys. Rev. Lett.* **101**, 026403 (2008).
- S9. Yang, J. *et al.*. Optical spectroscopy of superconducting $\text{Ba}_{0.55}\text{K}_{0.45}\text{Fe}_2\text{As}_2$: Evidence for strong coupling to low-energy bosons. *Phys. Rev. Lett.* **102**, 187003 (2009).
- S10. Drechsler S.-L. *et al.*. New insight into the physics of iron pnictides from optical and penetration depth data, *arXiv:0904.0827*.